ACS APPLIED MATERIALS & INTERFACES

Research Article

www.acsami.org

Intracellular pH-Sensitive Metallo-Supramolecular Nanogels for Anticancer Drug Delivery

Xuemei Yao,[†] Li Chen,*[,†] Xiaofei Chen,[†] Zhe Zhang,[†] Hui Zheng,[‡] Chaoliang He,*[,‡] Jingping Zhang,[†] and Xuesi Chen[‡]

[†]Department of Chemistry, Northeast Normal University, Changchun 130024, P. R. China

[‡]Key Laboratory of Polymer Ecomaterials, Changchun Institute of Applied Chemistry, Chinese Academy of Sciences, Changchun 130022, China

Supporting Information

ABSTRACT: For drug delivery systems, the most important factors are biocompatibility and stability. To achieve excellent biocompatibility, learning from naturally occurring systems may be the best choice. Herein, a series of pH-sensitive metallo-supramolecular nanogels (MSNs) were prepared by the metallo-supramolecular coordinated interaction between histidine and iron-*meso*-tetraphenylporphin, which mimicks the way that hemoglobin carries oxygen. With the excellent biocompatibility and special supramolecular pH sensitivity, MSNs had been exploited to load and release anticancer drug doxorubicin (DOX). In vitro drug release profiles showed that only a small amount of the loaded DOX was released in PBS solution at pH 7.4, while up to about 80% of the loaded DOX could be quickly released at pH 5.3 due to the pH-dependent disassembly of MSNs. Confocal laser scanning microscopy (CLSM) and flow cytometry were used to verify the cellular uptake and intracellular drug release behaviors of DOX-loaded MSNs toward MCF-7. Efficient cellular proliferation inhibition against MCF-7 and HeLa cells was also observed by a 3-(4,5-dimethyl-thiazol-2-yl)-2,5-diphenyl tetrazolium bromide (MTT) assay. These features suggested that MSNs could be of great potential as intelligent drug delivery systems.

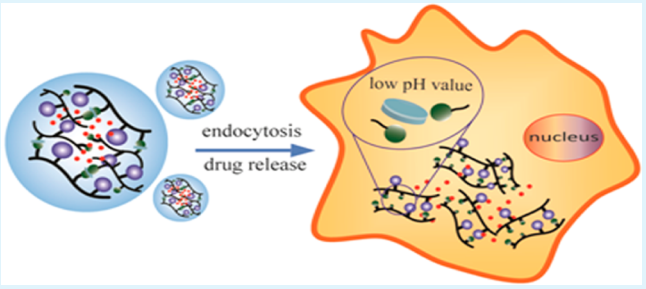

KEYWORDS: *metallo-supramolecular nanogels, intracellular pH-sensitive, dextran, histidine, iron-meso-tetraphenylporphin, drug delivery*

1. INTRODUCTION

Cancer is now the leading cause of morbidity and mortality in the world. In clinics, the principal cancer treatment is still chemotherapy.[1] However, many hydrophobic clinical antitumor drugs, such as doxorubicin (DOX) and paclitaxel (PTX), have limited clinical efficacy because of their low solubility, fragile stability, and the serious side effects caused by nonspecific biodistribution in the body. To solve these problems, the nanocarriers such as polymeric micelles, vesicles,[2,3] liposomes,[4,5] and nanogels[6] have been adopted to deliver antitumor drugs. Due to the accumulation in tumors via the electron paramagnetic resonance (EPR) effect, nanodrug delivery systems will improve the therapeutic efficiency and eliminate the adverse effects of the organism.

For a drug delivery system, its biocompatibility and stability in vivo are crucial factors. Coating materials may be a good strategy to improve the stability of the delivery system. Poly(ethylene glycol) (PEG) is the most commonly used coating material with nonfouling property.[7,8] PEGylated drug, protein, liposome, and nanoparticles had been studied widely and some had been used in clinical therapy or proceeded into the clinical phase. To achieve the best biocompatibility, learning about and choosing natural biocompatible materials such as proteins and polysaccharides as carriers may be the best way. Among these polysaccharides, dextran as a homopolysaccharide of glucose is similar to PEG. Due to its excellent biodegradability and nonfouling property, dextran has been widely used as a polymeric carrier.[9,10] Luo and co-workers constructed supramolecular microcapsules (SMCs) based on the self-assembly between polyaldenhyde dextran-graft-adamantane (PAD-*g*-AD) and carboxymethyl dextran-graft-β-CD (CMD-*g*-β-CD) on $CaCO_3$ particles via host−guest interaction. Then, SMCs were used to load adamantine-modified doxorubicin (AD-Dox) for cancer therapy.[11] Jin and coauthors designed a nanohybrid by $\pi-\pi$ interaction between nanoscale graphene oxide (NGO) and hematin-terminated dextran (HDex), which could effectively kill the drug-resistant MCF-7/ADR cells.[12] Compared with PEG, dextran is easier to modify because there are about 5% branching structure and abundant functional hydroxyl groups. The pH-sensitive

Received: February 21, 2014
Accepted: April 23, 2014
Published: April 23, 2014

   dx.doi.org/10.1021/am501093a | ACS Appl. Mater. Interfaces 2014, 6, 7816−7822

polymer acetylated dextran (Ac-DEX) with highly tunable degradation kinetics has been developed. The biocompatibility of acetylated dextran-type polymers has been enhanced, which has been used in high volume clinical applications such as multiple dosing and tissue engineering.[13]

The supramolecule plays an important role in naturally occurring systems such as various proteins driven by metallo-supramolecular assembly in vivo.[14−18] It is known that hemoglobin can efficiently carry oxygen driven by the metallo-supramolecular interaction between oxygen, iron-porphyrin, and histidine. Histidine exhibits pH-sensitive metallo-coordinated interaction with iron-porphyrin (Fe-Por).[19] At the physiological normal environment pH (∼7.4), two histidine moieties can bind to one Fe-Por via metallo-coordinated interactions. Under acidic conditions (pH < 6, the range of endosomal/lysosomal compartments), histidine will be protonated and the binding constant of histidine/Fe-Por will disassemble dramatically, resulting in the dissociation of Fe-Por from the histidine stalk. Taking advantage of this pH-sensitive metallo-supramolecular coordinated interaction, intracellular pH-responsive metallo-supramolecular nanogels based on dextran-*g*-cholesterol, histidine, and Fe-Por have been prepared. Dextran was chosen as the hydrophilic backbone due to its excellent biocompatibility and biodegradability. Cholesterol, as one of component of the cell membrane, is hydrophobic and beneficial to endocytosis.[20] The amphiphilic dextran-*g*-cholesterol copolymer was first synthesized and then modified by histidine. By the metallo-supramolecular coordinated interaction between histidine and Fe-Pro, intelligent MSNs have been successfully prepared finally. MSNs showed not only pH-sensitive property but also excellent biocompatibility and stability, hoping to be used as a potential drug deliverer for cancer therapy.

2. EXPERIMENTAL SECTION

2.1. Materials. Dextran (Dex, M_n = 40 kDa, Sigma), Boc-His-OH (Sigma), and cholesteryl chloroformate (98%, Sigma) were used directly. Doxorubicin hydrochloride (DOX·HCl) was bought from Zhejiang Hisun Pharmaceutical Co., Ltd. 3-(4,5-Dimethyl-thiazol-2-yl)-2,5-diphenyl tetrazolium bromide (MTT) was obtained from Sigma-Aldrich. Benzaldehyde, propionic acid, and pyrrole were bought from Aladdin, and pyrrole was used after distilling.

2.2. Characterizations. ^{1}H NMR spectra were collected on a Bruker AV 400 NMR spectrometer. Fourier transform infrared (FT-IR) measurements were performed on a Bio-Rad Win-IR spectrometer. Transmission electron microscopy (TEM) images were taken by a JEOL JEM-1011 transmission electron microscope. The size and distribution of particles were tested by a WyattQELS dynamic laser scattering (DLS) instrument. Confocal laser scanning microscopy (CLSM) was performed by Olympus FluoView 1000. A Bio-Rad 680 microplate reader was used to conduct MTT assay.

2.3. Synthesis of *meso*-Tetraphenylporphin (TPP). *meso*-Tetraphenylporphin (TPP) was prepared as in previous literature.[21,22] Freshly distilled pyrrole (80 mM, 5.6 mL) and benzaldehyde (80 mM, 8 mL) were added to propionic acid (300 mL). After refluxing for 30 min, the solution was cooled to room temperature and filtered, and then the filter cake was washed thoroughly with methanol. After washing using hot water, the resulting purple crystals were dried finally in vacuo to remove adsorbed water. Then the crude product was purified by recrystallization using chloroform ($CHCl_3$) and ethanol.

2.4. Synthesis of Iron-*meso*-tetraphenylporphin (Fe-Por). Iron-*meso*-tetraphenylporphin (Fe-Por) was synthesized according to the previous literature.[23] TPP (1.6 mM, 1 g) was dissolved in dimethylformamide (DMF), and $FeCl_2·4H_2O$ (6.5 mM, 1.3 g) was added three times over 30 min. Then the above mixture was refluxed, and the reaction process was monitored by thin-layer chromatography (TLC). The resulting mixture was cooled to 50∼60 °C, and then HCl was added to the mixture. After filtrating, the resulting solid was vacuum dried.

2.5. Synthesis of Dextran-*g*-cholesterol (DC). Dex (0.025 mM, 1 g) and triethylamine (TEA) (1.2 mM, 0.2 mL) were dissolved in dry 20 mL of dimethyl sulfoxide (DMSO) in a flask under N_2 protection at 25 °C. Cholesteryl chloroformate (0.6 mM, 0.28 g) was dissolved in dry 10 mL of chloroform ($CHCl_3$) and added dropwise slowly into the solution. The reaction was stirred at 0 °C for 48 h. After removing $CHCl_3$, the solution was dialyzed against deionized water for 3 days, and the product was collected by lyophilization.

2.6. Synthesis of Boc-His-OH Modified Dextran-*g*-cholesterol (HDC). DC (0.02 mM, 1 g), Boc-His-OH (1.5 mM, 0.37 g), 1-ethyl-3-(3-dimethyllaminopropyl) carbodide hydrochloride (EDC·HCl) (3.0 mM, 0.57 g), and 4-dimethylaminopyridine (DMAP) (0.3 mM, 0.04 g) were added into 20 mL of DMSO in a glass flask. Then the solution was stirred at 25 °C for 48 h. The solvent and unreacted substances were removed by dialysis against deionized water for 72 h. The solution was lyophilized.

2.7. Synthesis of pH-Sensitive Metallo-Supramolecular Nanogels (MSNs). HDC (0.0035 mM, 0.5 g) and Fe-Por (0.5 mM, 0.4 g) were dissolved in 10 mL of DMSO. The mixture was stirred at 25 °C for 48 h. Then, the solvent and unreacted substances were removed by dialysis against deionized water for 72 h. The products were obtained by lyophilization.

2.8. In Vitro Drug Loading, Release, and Cell Assay. In vitro drug loading, release, and cell assay experiments were preformed according to our earlier work.[24] The detailed procedure could be found in the Supporting Information.

3. RESULTS AND DISCUSSION

3.1. Preparation and Characterization of *meso*-Tetraphenylporphin (TPP). *Meso*-tetraphenylporphin (TPP) was synthesized as in previous literature[21,22] as shown in Scheme S1A (Supporting Information). The chemical structures of TPP were characterized by ^{1}H NMR, FT-IR, UV−vis, and elemental analysis. As shown in Figure S1 (Supporting Information), the peaks at 8.9 ppm (1), 8.2 ppm (2), and 7.9 ppm (3, 4) and −2.7 ppm (5) assigned to TPP indicated the successful synthesis of TPP. In addition, the peaks at 2.7 ppm betrayed the formation of the porphyrin macrocycle. FT-IR analysis of TPP was also conducted (Figure S2, Supporting Information). The peaks appearing at 3038, 3060, and 3316 cm^{-1} further suggested the successful synthesis of TPP. The peaks at 3316 cm^{-1} assigned to N−H also demonstrated the structure of a porphyrin macrocycle. The UV−vis spectrum of TPP was shown in Figure S3A (Supporting Information). There the peaks appearing at 412 nm (1), 514 nm (2), 550 nm (3), 590 nm (4), and 644 nm (5) also confirmed the structure of TPP. The elemental analysis of TPP was also conducted with a result of N (%) 2.1490, C (%) 85.90, and H (%) 4.952. All of these results suggested the successful synthesis of TPP.

3.2. Preparation and Characterization of Iron-*meso*-tetraphenylporphin (Fe-Por). Iron-*meso*-tetraphenylporphin (Fe-Por) was synthesized according to the previous literature[23] as shown in Scheme S1B (Supporting Information). The chemical structure of Fe-Por was confirmed by UV−vis. As shown in Figure S3B (Supporting Information), the UV−vis spectrum of Fe-Por was different from that of free base TPP. Compared with free base TPP, some peaks at the Q-band of Fe-Pro disappeared, and the peaks at the S band had slightly shifted. The change of the UV−vis indicated the successful synthesis of TPP.

3.3. Preparation and Characterization of Histidine-Modified Dextran-*g*-cholesterol (HDC). Herein, histidine-

modified dextran-*g*-cholesterol (HDC) was synthesized as shown in Scheme S1C (Supporting Information). The chemical structures of HDC were assured by ^{1}H NMR and FT-IR. As shown in Figure 1, the peak appearing at 5.8 ppm (11) was

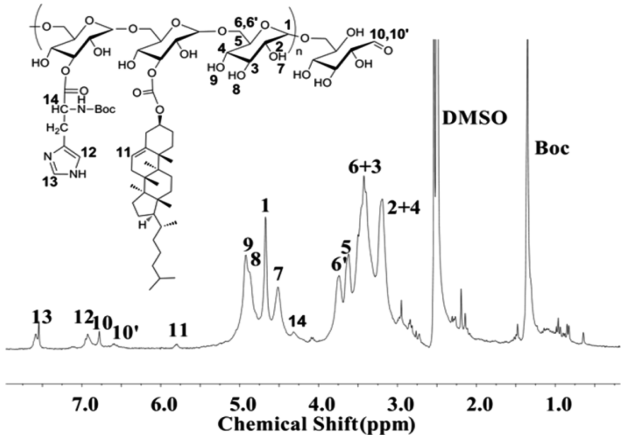

Figure 1. ^{1}H NMR spectrum of HDC in DMSO-d_6.

assigned to cholesterol, and the peaks at 6.9 ppm (12), 7.6 ppm (13), 4.3 ppm (14), and 1.4 ppm (Boc) that belonged to histidine demonstrated the successful synthesis of HDC. FT-IR analysis of HDC also acted as shown in Figure 2A. The peaks at

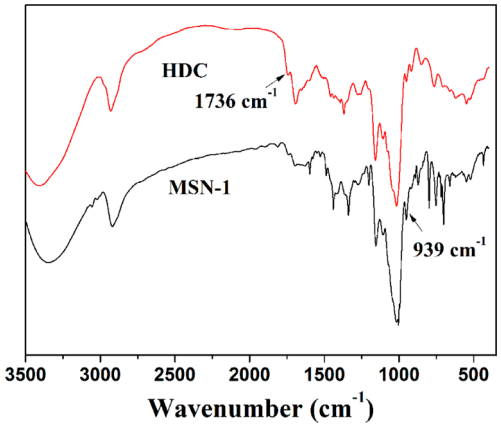

Figure 2. FT-IR spectra of HDC and MSN-1.

1736 cm^{-1} assigned to HDC further indicated the successful synthesis of HDC. The grafted ratios were calculated by the integration ratio between the protons of hydroxyl groups from dextran appearing at 4.5 ppm and the peak of cholesterol appearing at 6.0 ppm and the peak of histidine appearing at 8.2 ppm in Figure 1, according to the following eq 1

$$\text{grafting ratios of hydroxyl groups (mol \%)} = I_{11}(I_{12})/I_7 \times 100 \quad (1)$$

The grafting ratios of cholesterol and histidine were 12% and 28%, respectively.

3.4. Preparation and Characterization of Metallo-Supramolecular Nanogels (MSNs). MSNs were prepared as shown in Scheme 1. By adjusting the feed ratio, we synthesized MSN-1 and MSN-2 as listed in Table S1 (Supporting Information). The chemical structures of MSNs were confirmed by FT-IR and UV−vis. As shown in Figure 2, the peak at 939 cm^{-1} was assigned to Fe−N on MSNs. As seen from in Figure S3C (Supporting Information), the UV−vis spectrum of MSNs changed obviously which is completely different from that of Fe-Por. These results indicated the successful preparation of MSNs.

To confirm the self-assembly of MSNs, Nile Red was used as a probe to investigate the critical micelle concentration (CMC) value.[25] Tracking the fluorescence intensity of Nile Red as a function of MSN concentration, the CMC could be calculated. Expectedly, the fluorescence intensity increased with the enlargement of MSN concentration. As listed in Table S1 (Supporting Information), the CMC values were impacted by the cross-linking ratios of MSNs. Following the increasing cross-linking ratios of MSN, the CMC value was investigated and became lower, which implied that the hydrophobicity of MSNs would increase.

The size of MSNs in PBS at different pH value was monitored by DLS measurement and TEM (Figure 3) to further certify the pH-sensitivity. Notably, the R_h values of MSN-1 gradually increased from 78 ± 10 to 233 ± 118 nm because of the disassembly between histidine and Fe-Por at lower pH value. As shown in Figure 3B and C, both the size and the polydispersity index (PDI) of MSN-1 tend to be larger at pH 5.3 than at pH 7.4. It was attributed to the decrease of hydrophobicity resulting from the disassembly of Fe-por and histidine.

Scheme 1. Synthetic Route for MSNs

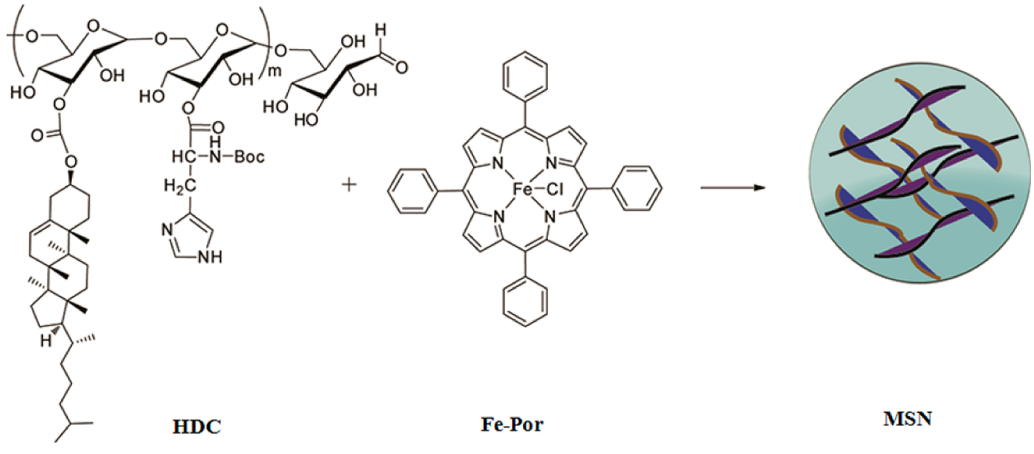

dx.doi.org/10.1021/am501093a | ACS Appl. Mater. Interfaces 2014, 6, 7816−7822

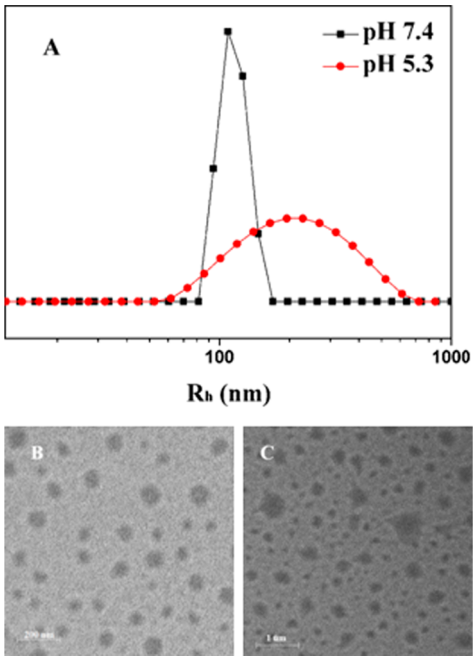

Figure 3. Hydrodynamic radii (R_h) of MSN-1 in PBS at pH 7.4 and pH 5.3 (A). TEM micrographs of MSN-1 at pH 7.4 (B) and pH 5.3 (C), respectively.

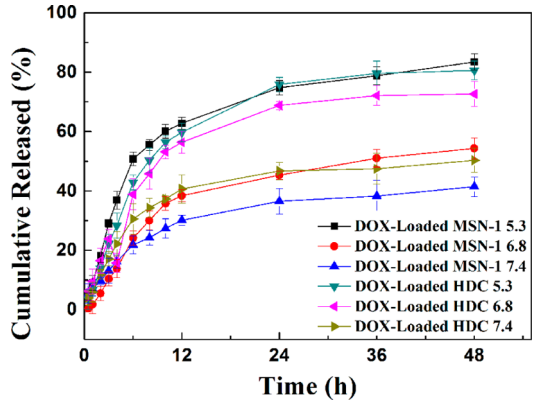

Figure 4. In vitro DOX release profiles for DOX-loaded MSN-1 and HDC in PBS at 37 °C at pH 5.3, 6.8, and 7.4, respectively.

3.5. In Vitro DOX Loading and Triggered Release. Doxorubicin (DOX), a kind of antineoplastic drug, is commonly used in the therapy of cancers, such as cervical cancer, leukemia, lung cancer, liver cancer, and so on. Herein, to demonstrate the feasible application of the pH-sensitive MSNs for antitumor drug delivery, DOX was entrapped into MSNs as a model drug (Scheme 2). The drug loading content (DLC) of MSN-1 and MSN-2 were 4.63% and 7.32%, respectively, while the DLC of HDC was 3.21% as listed in Table S1 (Supporting Information). The result verified that the DLC was enlarged after the assembly between histidine and Fe-Por. The in vitro release behaviors were performed at pH 5.3, 6.8, and 7.4, respectively. A desirable release profile of DOX loaded in HDC and MSN-1 versus time is described in Figure 4. The cumulative release percentage of DOX from DOX-loaded HDC and MSN-1 reached to about 80% in PBS at pH 5.3 in 48 h, while the DOX release rate of MSN-1 was obviously lower at pH 7.4 than that of HDC. This indicated that MSNs were more stable than the HDC micelle at pH 7.4. Further, the DOX release rate at pH 5.3 was obviously higher than at pH 7.4, which was rooted in the disassembly of MSN at low pH value. These phenomena implied that MSNs could effectively conceal the release of the loaded drug in normal physiological environments while improving the drug release in answer to lower pH value at the cancer cell. These properties imply that pH-sensitive MSNs have great capacity for drug delivery for antitumor drugs.

3.6. Intracellular DOX Release and Cellular Proliferation Inhibition. CLSM and flow cytometry were used to detect the cellular uptake and intracellular drug release behaviors of DOX-loaded MSNs in MCF-7 cells. After incubation with MSNs for 2 h, the intracellular red fluorescence was not discovered in the MCF-7 cells (Figure 5A). Intracellular DOX fluorescence in cells incubated with DOX-loaded MSN-1 was higher than that incubated with DOX-loaded DC (Figure 5D and A), which was ascribed to the disassembly of MSN-1 response to lower pH in cancer cells. On the contrary, the fluorescence intensity of DOX incubated with DOX-loaded HDC was slightly different from that incubated with DOX-loaded MSN-1 because of the pH sensitivity of HDC (Figure 5C and D). Compared with cells treated with DOX alone, the DOX fluorescence in cells incubated with DOX-loaded MSN-1 was similar (Figure 5D and Figure S4, Supporting Information). As shown in Figure 6A and 6B, along with the increase of incubation time with DOX-loaded MSN-1, the intracellular DOX fluorescence intensity tended to be higher. In addition, compared with cells incubated for 2 h, the fluorescence intensity of DOX in cells incubated for 24 h had little difference, which may be attributed to the stability of MSNs. Flow cytometric analyses were also used to monitor drug release triggered by the intracellular environment. As shown in Figure 7B, the flow cytometric histogram for the cells

Scheme 2. Schematic Illustration of DOX Loading and Intracellular Microenvironment Triggered Release from DOX-Loaded MSNs

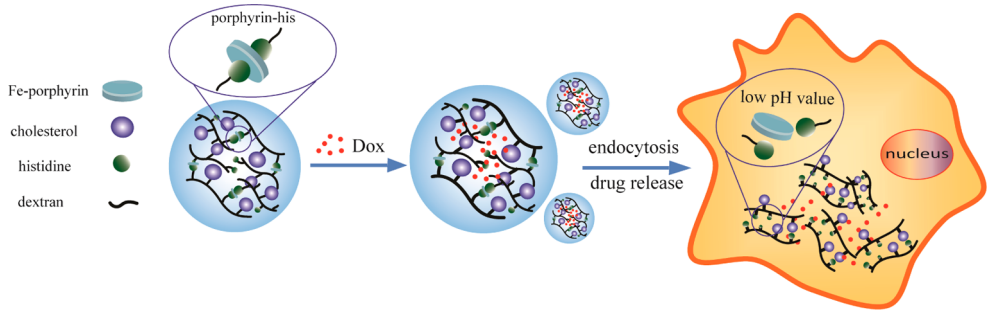

dx.doi.org/10.1021/am501093a | ACS Appl. Mater. Interfaces 2014, 6, 7816−7822

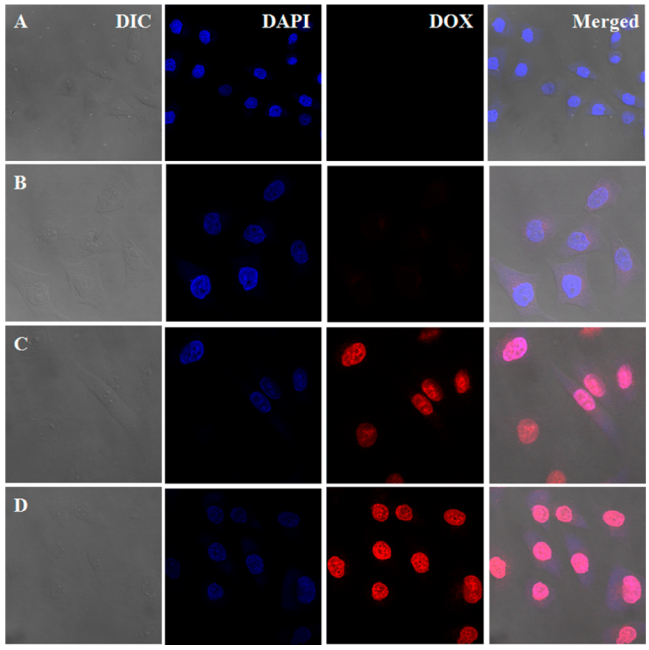

Figure 5. Representative CLSM images of MCF-7 cells incubated with MSN-1 (A), DOX-loaded DC (B), DOX-loaded HDC (C), and DOX-loaded MSN-1 (D) for 2 h. For each panel, the images from left to right show a differential interference contrast (DIC) image, cell nuclei stained by DAPI (blue), DOX fluorescence in cells (red), and overlays of the three images.

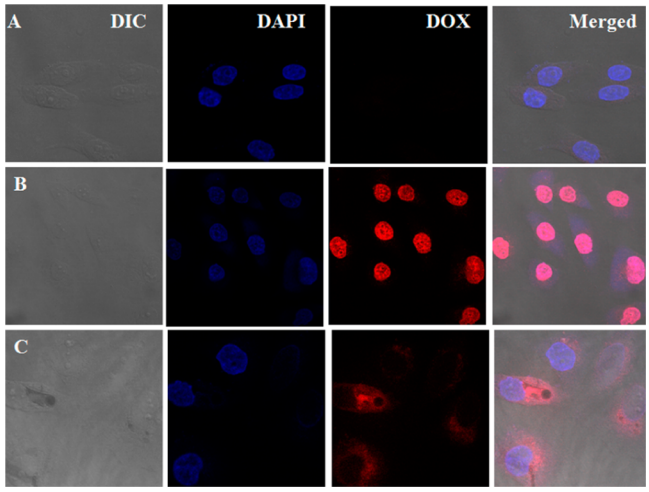

Figure 6. Representative CLSM images of MCF-7 cells incubated with DOX-loaded MSN-1 for 15 min (A), 2 h (B), and 24 h (C). For each panel, the images from left to right show a differential interference contrast (DIC) image, cell nuclei stained by DAPI (blue), DOX fluorescence in cells (red), and overlays of the three images.

incubated with DOX-loaded MSN-1 transferred obviously to the high fluorescence intensity position. The clear observation of DOX fluorescence within the MCF-7 cells may be attributed to a pH-triggered disassembly of MSN-1.

The in vitro cytotoxicity of MSNs toward MCF-7 and HeLa cells was estimated using a MTT assay. As shown in Figures S5 and S6 (Supporting Information), the viabilities of MCF-7 and HeLa cells which were incubated with MSNs for 72 h were over 85% at all test concentrations, even as high as 10 g L^{-1}. This was proof that MSNs were biocompatible and slightly cytotoxic to cells.

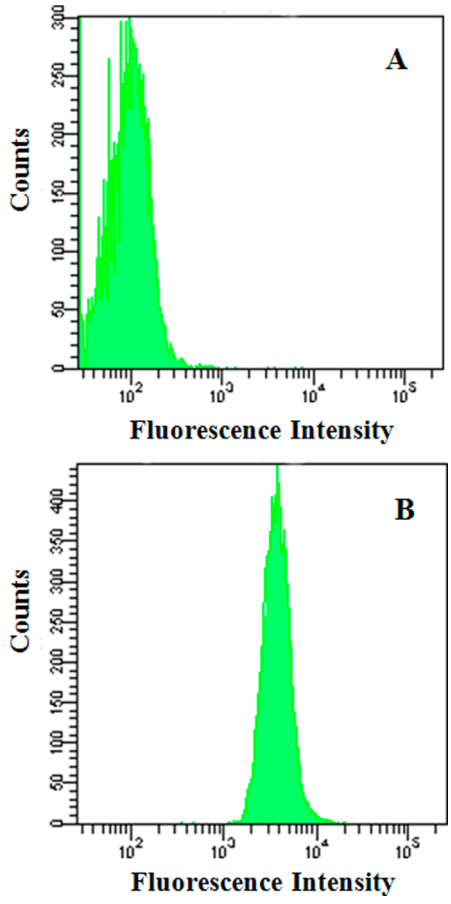

Figure 7. Flow cytometry profiles of MCF-7 cells incubated with PBS (A) and MSN-1 (B) for 2 h.

MTT assay was also used to evaluate in vitro cytotoxicity of DOX-loaded MSN-1 toward MCF-7 and HeLa cells. As shown in Figure 8 and Figure S7 (Supporting Information), DOX-loaded MSN-1 betrayed obvious cytotoxicities to both MCF-7 and HeLa cells at 24, 48, and 72 h, which were slightly lower than those of free DOX. These results certified that DOX release from the DOX-loaded MSN-1 may be triggered by the acidic endosomal microenvironment, which demonstrated the MSNs had a promising application as intelligent drug delivery agents.

CONCLUSION

In summary, mimicking the way that hemoglobin carries oxygen, a series of pH-responsive metallo-supramolecular nanogels were successfully fabricated by the metallo-supramolecular coordinated interaction between histidine and iron-*meso*-tetraphenylporphin. MSNs showed excellent intracellular pH-sensitivity and could be used as an intelligent drug delivery agent. The acid-sensitive metallo-supramolecular nanogels were researched for rapid intracellular release of doxorubicin (DOX). The DOX release from DOX-loaded MSNs was sped up in acid environments triggered by the endosomal/lysosomal conditions. The strong intracellular DOX release was discovered in MCF-7 cells. DOX-loaded MSNs displayed high cellular proliferation inhibition toward MCF-7 and HeLa. Therefore, with the excellent biocompatibility and stability, MSNs could act as a potential smart platform for drug delivery system.

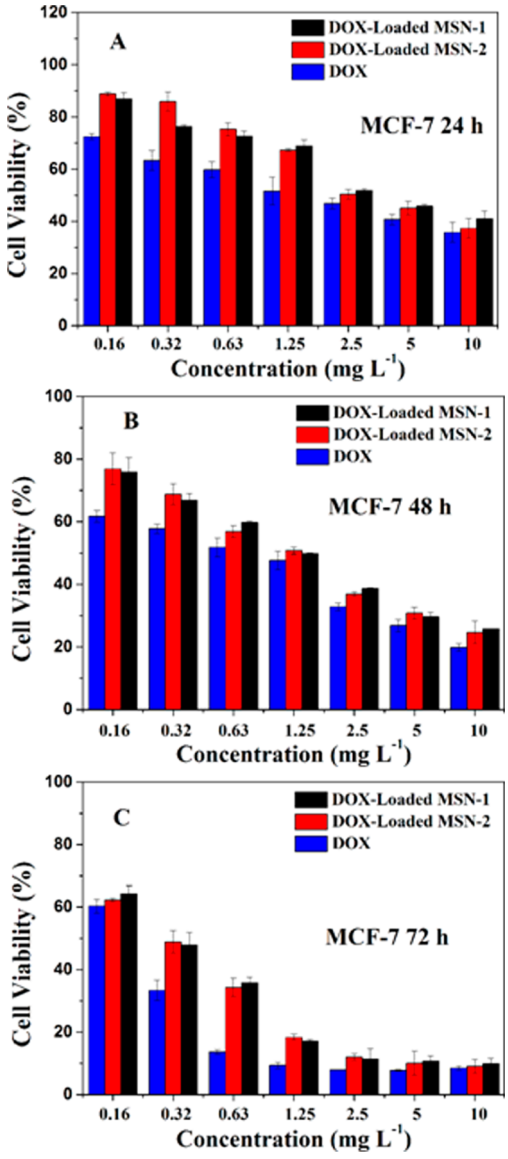

Figure 8. Cytotoxicity of DOX-loaded MSN-1 and MSN-2 toward MCF-7 cells after incubation for 24 h (A), 48 h (B), and 72 h (C).

■ ASSOCIATED CONTENT

Supporting Information

Additional experimental sections and characterization data are provided. This material is available free of charge via the Internet at http://pubs.acs.org.

■ AUTHOR INFORMATION

Corresponding Authors

*Tel.: +86 431 85099667. Fax: +86 431 85099668. E-mail: chenl686@nenu.edu.cn

*E-mail: clhe@ciac.ac.cn.

Notes

The authors declare no competing financial interest.

■ ACKNOWLEDGMENTS

This research was financially supported by the National Natural Science Foundation of China (Projects 51273037, 50903012, and 21174142), Jilin Science and Technology Bureau (20130206074GX, International Cooperation Project 20120729), Jilin Human Resources and Social Security Bureau (201125020), and Jilin Environmental Protection Bureau (201127).

■ REFERENCES

(1) Swift, L. P.; Rephaeli, A.; Nudelman, A.; Phillips, D. R.; Cutts, S. M. Doxorubicin-DNA Adducts Induce a Non-Topoisomerase II-Mediated Form of Cell Death. *Cancer Res.* **2006**, *66*, 4863−4871.

(2) Yuk, S. H.; Oh, K. S.; Koo, H.; Jeon, H.; Kim, K.; Kwon, I. C. Multi-core Vesicle Nanoparticles Based on Vesicle Fusion for Delivery of Chemotherapic Drugs. *Biomaterials* **2011**, *32*, 7924−7931.

(3) Yang, X.; Grailer, J. J.; Rowland, I. J.; Javadi, A.; Hurley, S. A.; Matson, V. Z.; Steeber, D. A.; Gong, S. Multifunctional Stable and pH-Responsive Polymer Vesicles Formed by Heterofunctional Triblock Copolymer for Targeted Anticancer Drug Delivery and Ultrasensitive MR Imaging. *ACS Nano* **2010**, *4*, 6805−6817.

(4) Du, Y.; Chen, W.; Zheng, M.; Meng, F.; Zhong, Z. pH-Sensitive Degradable Chimaeric Polymersomes for the Intracellular Release of Doxorubicin Hydrochloride. *Biomaterials* **2010**, *31*, 7575−7585.

(5) Bochot, A.; Fattal, E. Liposomes for Intravitreal Drug Delivery: A State of the Art. *J. Controlled Release* **2012**, *161*, 628−634.

(6) Ding, J.; Shi, F.; Xiao, C.; Lin, L.; Chen, L.; He, C.; Zhuang, X.; Chen, X. One-step Preparation of Reduction-responsive Poly (Ethylene Glycol)-Poly (Amino Acid) s Nanogels as Efficient Intracellular Drug Delivery Platforms. *Polym. Chem.* **2011**, *2*, 2857−2864.

(7) Calvo, P.; Gouritin, B.; Chacun, H.; Desmaële, D.; D'Angelo, J.; Noel, J.-P.; Georgin, D.; Fattal, E.; Andreux, J. P.; Couvreur, P. Long-Circulating PEGylated Polycyanoacrylate Nanoparticles as New Drug Carrier for Brain Delivery. *Pharm. Res.* **2001**, *18*, 1157−1166.

(8) Langer, R. Drugs on Target. *Science* **2001**, *293*, 58−59.

(9) Liu, Z.; Jiao, Y.; Wang, Y.; Zhou, C.; Zhang, Z. Polysaccharides-based Nanoparticles as Drug Delivery Systems. *Adv. Drug Delivery Rev.* **2008**, *60*, 1650−1662.

(10) Österberg, E.; Bergström, K.; Holmberg, K.; Schuman, T. P.; Riggs, J. A.; Burns, N. L.; Van Alstine, J.; Harris, J. M. Protein-Rejecting Ability of Surface-Bound Dextran in End-On and Side-On Configurations: Comparison to PEG. *J. Biomed. Mater. Res.* **1995**, *29*, 741−747.

(11) Luo, G.-F.; Xu, X.-D.; Zhang, J.; Yang, J.; Gong, Y.-H.; Lei, Q.; Jia, H.-Z.; Li, C.; Zhuo, R.-X.; Zhang, X.-Z. Encapsulation of an Adamantane-Doxorubicin Prodrug in pH-Responsive Polysaccharide Capsules for Controlled Release. *ACS Appl. Mater. Interfaces* **2012**, *4*, 5317−5324.

(12) Jin, R.; Ji, X.; Yang, Y.; Wang, H.; Cao, A. Self-Assembled Graphene-Dextran Nanohybrid for Killing Drug-Resistant Cancer Cells. *ACS Appl. Mater. Interfaces* **2013**, *5*, 7181−7189.

(13) Kauffman, K. J.; Do, C.; Sharma, S.; Gallovic, M. D.; Bachelder, E. M.; Ainslie, K. M. Synthesis and Characterization of Acetalated Dextran Polymer and Microparticles with Ethanol as a Degradation Product. *ACS Appl. Mater. Interfaces* **2012**, *4*, 4149−4155.

(14) Yu, G.; Ma, Y.; Han, C.; Yao, Y.; Tang, G.; Mao, Z.; Gao, C.; Huang, F. A Sugar-Functionalized Amphiphilic Pillar [5] Arene: Synthesis, Self-Assembly in Water, and Application in Bacterial Cell Agglutination. *J. Am. Chem. Soc.* **2013**, *135*, 10310−10313.

(15) Yao, Y.; Xue, M.; Chen, J.; Zhang, M.; Huang, F. An Amphiphilic Pillar [5] Arene: Synthesis, Controllable Self-Assembly in Water, and Application in Calcein Release and TNT Adsorption. *J. Am. Chem. Soc.* **2012**, *134*, 15712−15715.

(16) Ge, Z.; Liu, S. Facile Fabrication of Multistimuli-Responsive Metallo-Supramolecular Core Cross-Linked Block Copolymer Micelles. *Macromol. Rapid Commun.* **2013**, *34*, 922−930.

(17) Chisholm, M. H.; Choojun, K.; Chow, A. S.; Fraenkel, G. Molecular Dynamics and Ligand Exchange in Magnesium Complexes: Evidence for both Dissociative and Associative Ligand Exchange. *Angew. Chem., Int. Ed.* **2013**, *52*, 3264−3266.

(18) Zhang, K.; Zha, Y.; Peng, B.; Chen, Y.; Tew, G. N. Metallo-Supramolecular Cyclic Polymers. *J. Am. Chem. Soc.* **2013**, *135*, 15994−15997.
(19) Kobayashi, Y.; Takashima, Y.; Hashidzume, A.; Yamaguchi, H.; Harada, A. Reversible Self-Assembly of Gels through Metal-Ligand Interactions. *Sci. Rep.* **2013**, *3*, 1243.
(20) Janout, V.; Zhang, L.-h.; Staina, I. V.; Di Giorgio, C.; Regen, S. L. Molecular Umbrella-Assisted Transport of Glutathione across a Phospholipid Membrane. *J. Am. Chem. Soc.* **2001**, *123*, 5401−5406.
(21) Adler, A. D.; Longo, F. R.; Finarelli, J. D.; Goldmacher, J.; Assour, J.; Korsakoff, L. A Simplified Synthesis for Meso-Tetraphenylporphine. *J. Org. Chem.* **1967**, *32*, 476−476.
(22) Luguya, R.; Jaquinod, L.; Fronczek, F. R.; Vicente, M. G. H.; Smith, K. M. Synthesis and Reactions of Meso-(p-Nitrophenyl) Porphyrins. *Tetrahedron* **2004**, *60*, 2757−2763.
(23) Sun, Z.; She, Y.; Zhong, R. Synthesis of p-Substituted Tetraphenylporphyrins and Corresponding Ferric Complexes with Mixed-Solvents Method. *Front. Chem. Eng. China* **2009**, *3*, 457−461.
(24) Zhang, Z.; Chen, X.; Chen, L.; Yu, S.; Cao, Y.; He, C.; Chen, X. Intracellular pH-Sensitive PEG-block-Acetalated-Dextrans as Efficient Drug Delivery Platforms. *ACS Appl. Mater. Interfaces* **2013**, *5*, 10760−10766.
(25) Zhang, A.; Zhang, Z.; Shi, F.; Ding, J.; Xiao, C.; Zhuang, X.; He, C.; Chen, L.; Chen, X. Disulfide Crosslinked PEGylated Starch Micelles as Efficient Intracellular Drug Delivery Platforms. *Soft Matter* **2013**, *9*, 2224−2233.